Mineralogical and Geochemical Variations in Ferro-manganese Nodules from Campbell Drift

Se Won Chang*, Hunsoo Choi, Sung-Rock Lee
(swchang@kigam.re.kr)
Petroleum & Marine Resources Research Division,
Korea Institute of Geoscience & Mineral Resources(KIGAM)

Introduction

This is a part of the joint KIGAM-GNS-NIWA 3-year study of ferro-manganese nodules on the Campbell Drift, east of Campbell Plateau to determine age distribution, growth rates and geochemical evolution in relation to geographic setting.

SAA3 cruise in July-August 1999 by *RV Tangaroa* along the southern and eastern margins of the Campbell Plateau yielded more than 4000 nodules, ranging in size from <2~40cm by twelve successful dredges across two transects. The nodule occurrences in the region can be classified into six facies, by comparing the collected samples and the seafloor photographs. Six nodule facies can be assigned as facies RH, DH, IB, HH, DL and HB (Fig. 1&2).

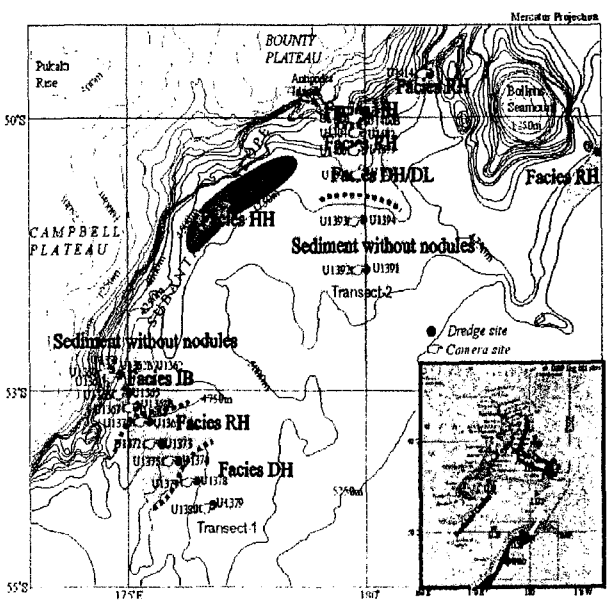

Fig. 1. Position map of camera and dredge, and dominant nodule facies distribution.

The most distinct and dominant facies in this area is facies RH, consisting of large nodules with round shape. The nodule coverage of the RH facies may be over than 50% and the nodule size may change. In addition, it contains rock boulders. The characteristic nodule types comprising facies RH are E_{bt}^{bs} and D_{bt}^{bs} of dredge U1373, and various U type nodules, such as, U_{br}^{bt} of dredge U1399, $U_{r\text{-}b}^{t}$ of U1402, U_{s}^{s} of U1406B, and U_{b}^{t} of U1413, ranging 6~20cm in long diameter. Facies DH consists of small nodules of variable size and shape,

probably of early diagenetic origin, and has a high nodule density. The samples taken up by dredge U1374, U1398, and U1402 are mainly composed of facies DH nodules. The frequent nodule types of facies DH are S_b, E_b, P_b, I_b, and D_b^{r-b}, ranging 2~12cm in long diameter. The nodules of dredge U1373 and U1399 are mixed with facies DH and RH. D_b, D_b^t, T_{b-r}, T_t, I_{r-b}, I_r, I_{t-r}, P_r, P_{b-r}, and P_t types also occur in places. Facies IB consists of large nodules and boulders of irregular shape. The characteristic nodule types are large I_{t-b}^b or I_{t-b}^s, and S_b^s types, ranging in size from 15~30cm, of dredge U1365B. The nodules comprising facies HH have smooth surfaces, but show variable size and shape. Facies HH has a high nodule density, probably of hydrogenetic origin. The most dominant nodule types are S_s, E_s, P_s, and I_s, less than 10cm in size, of dredge U1406B. The occurrence of facies DL suggests that the nodule types are similar to those of facies DH, but have medium to low density. The nodules of dredge U1398 may contain the nodule types of facies DL, such as, S_b, E_b, P_b, I_b, and D_b^{r-b} types, ranging 2~12cm in long diameter. Facies HB consists of mainly large nodules with smooth surfaces, probably of hydrogenetic origin, associated with some large rock boulders encrusted with thin ferromanganese oxides. The seafloor photographs of facies HB are generally indistinguishable with those of facies RH, but facies HB shows distinct bimodal distribution of nodules with more boulders than facies RH. The dredge U1406B and U1413 are composed of facies HB nodules. The frequent nodule types of facies HB are P_s, U_s or U_b^t, S_s or S_{t-b}, and E_s, ranging 2~30cm in long diameter, and boulders of B_b^s, B_t or B_{r-t} type occur together. Small amounts of I_s, I_b, and T_t type less than 8cm in long diameter occur as well.

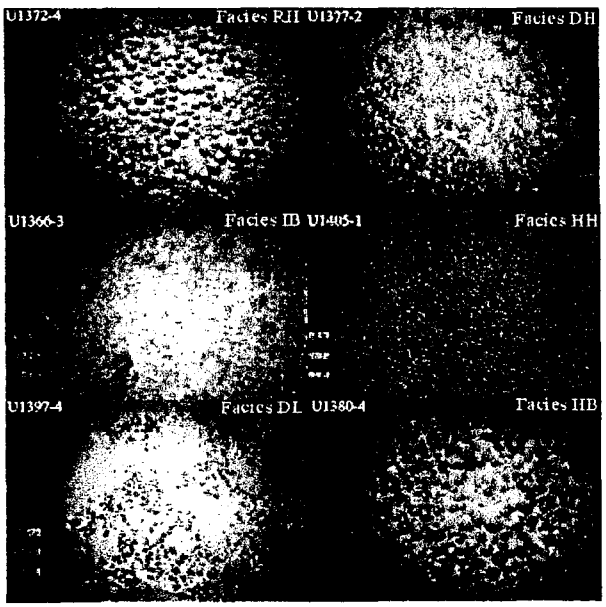

Fig. 2. Various facies of nodule occurrence.

Methods of Study

Four nodule samples were selected and polished sections were prepared to observe the internal textures under the optical and electron microscope. Back-scattered electron images (BEI) were taken to present the whole sequences of growth texture and electron probe micro analyses (EPMA) were done. The chemical compositions and mineralogical compositions were analyzed for the sub-samples divided by each internal textural zone of the nodule samples.

U1373-2 nodule was divided into 11 internal textural zones, U1398-1 into 6 zones, U1402-1 into 10 zones, and U1406B-2 into 12 zones (Fig. 3). Distances of the each zone from the surface were measured (Table 1).

Powder samples prepared for chemical analysis were analyzed by X-ray diffractometer under the room temperature first. The same mounted samples were heat-treated in the electric oven at 105°C during overnight, then analyzed secondly.

The major elements, such as, MnO_2, Fe_2O_3, SiO_2, TiO_2, Al_2O_3, MgO, CaO, Na_2O, K_2O, and P_2O_5, were analyzed by XRF. U, Th, Y, and the rare earth elements were analyzed by ICP-mass. The other minor and trace elements were analyzed by ICP. All analyses were done after drying overnight at 105°C. The Be^{10} and Be^9 contents were analyzed at the institute of Geological & Nuclear Sciences (GNS) in New Zealand, then the growth rates and the ages of the boundary between each textural zone were calculated from the Be^{10}/ Be^9 ratios (Table 1).

Results

Mineralogy

The major Mn-Fe oxyhydroxide minerals are vernadite and buserite. Vernadites are found in all of the textural zones, but buserites are found only in U1398-1 nodule and zone 1, 4, 5&6 of U1402-1 nodule. The other major and minor minerals are quartz, feldspar, pyroxene, amphibole, ilmenite, apatite, mica and berthierine (Table 1).

Hierarchical cluster analysis based on the correlation coefficient was done for the hygroscopic water(H_2O^-)-free chemical compositions of 39 subsamples except for Be & SiO_2, n=25. The elements grouped by hierarchical cluster analysis are assigned to following four phases, which are essentially similar to those interpreted from the correlation coefficients.

REEs, U, Th, P_2O_5, TiO_2, and Fe_2O_3 have strong positive correlation and make Fe_2O_3 group. Co, Zr, and Be have also strong positive correlation and make Co group. There is also weak positive correlation between Fe_2O_3 group and Co group. Fe_2O_3 group and Co group may be originated from same **Fe-rich phase** probably of terrestrial detritals. MnO_2, CO_2, and H_2O make MnO_2 group. Cu, Zn , Ni, MgO and Mo compose also Cu group. There is a weak positive correlation between MnO_2 group and Cu group. MnO_2 group and Cu group may be originated from same phase, **Mn-oxyhydroxide**. SiO_2, Al_2O_3, Sc, and K_2O have strong positive correlation and make SiO_2 group. SiO_2 group may be originated from **silicate** phase. Sr, V, Ba, Pb, and As compose Ba group and may be originated from **sulfate** phase, probably of biogenic source.

Hierarchical cluster analysis based on the correlation coefficient was also done for the 318 electron microprobe data except for Cl, n=210. The elements grouped by hierarchical cluster

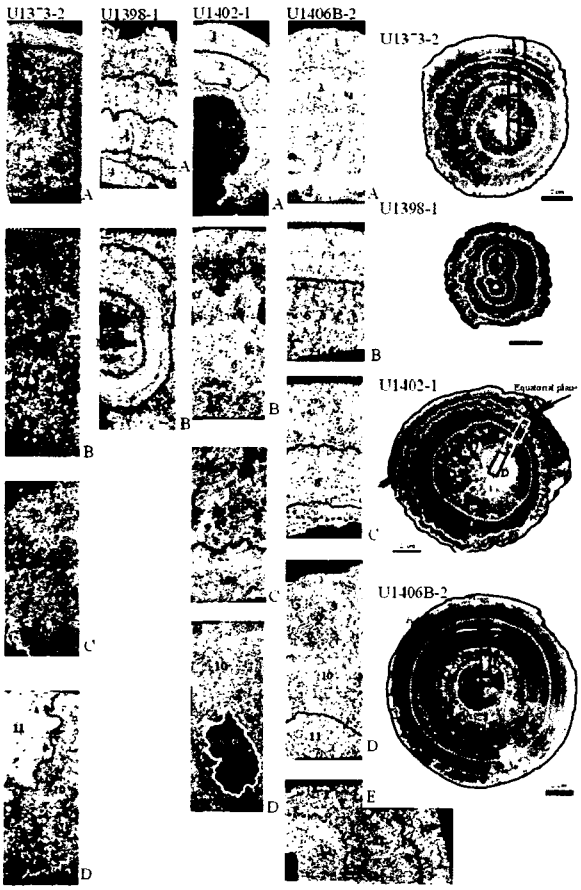

Fig. 3. Back-scattered electron images and analyzed positions of the nodules

analysis are assigned to following five phases. Mn, Ni, Cu, Mg, Na, Zn have strong positive correlation and make Mn group, originated from **Mn-oxyhydroxide** minerals, such as, vernadite and buserite. Si, Al, Cl, and K have also strong positive correlation and make Si group, originated from **Al-silicate** minerals. Ti, V, and Fe make Fe group, probably originated from **Fe-rich** minerals. Ca and P compose Ca group, that is, **phosphate**. There is a weak positive correlation between Fe group, Ca group, and Co. Ba and Pb make Ba group, originated from **sulfate** probably of biogenic source.

Variations of chemical compositions versus Mn/Fe

The contents of the major, minor, and trace elements against Mn/Fe ratios for each textural zone were plotted. CaO, MgO, Cu, Ni, and Zn show positive correlations, even though CaO, Cu, and Ni contents can be divided into two groups showing highly positive correlations and weakly positive correlations. Co can be also divided into two groups showing highly positive correlations and rather uniform contents. Whereas, P_2O_5, TiO_2, Sc, Zr, Y, Th, U, total REEs, and Be show negative correlations. SiO_2, Al_2O_3 and K_2O contents also can be divided into two groups showing negative correlations and rather uniform contents. Na_2O and As show rather uniform contents. Ba, Sr, and V show very weak correlations, but three kinds of correlations can be recognized, that is, U1402-1 nodule show positive correlations, but the others show negative correlations with higher contents or lower contents. As, Pb, Ce/La and LREE/HREE belongs to rather narrow range regardless of Mn/Fe.

Normalized REE patterns

The contents of the rare earth elements for each textural zone were normalized by NACS (North America Continental Shale). Compared to the REE data of nodules and crusts from Northeast Pacific and Southeast Pacific (Schreiber, 1981), the NACS normalized REE patterns

of the nodules in this study match with the range of Northeast Pacific crusts and nodules. However, the patterns show much higher values than those of diagenetic nodules from Southeast Pacific. All data show positive Ce anomaly and are plotted between the range of hydrogenetic and early diagenetic type nodules, although the values of each zone are variable even in one nodule (Table 1). Each textural zone might be assigned to three kinds of growth mechanism by microscopic textures and NACS normalized REE patterns, even though the mechanism is not quite certain in cases.

For U1373-2 nodule, zone 1, 2, 3, 7, 8, and 9 belong to the range of hydrogenetic growth, whereas, zone 4, 5, 6, 10, and 11 belong to the range of mixed origin between hydrogenetic growth and early diagenetic growth. For U1398-1 nodule, zone 1 and 2 belong to the range of early diagenetic growth, whereas, zone 3, 4, 5, and 6 belong to the range of mixed origin between hydrogenetic growth and early diagenetic growth. For U1402-1 nodule, zone 1, 2, and 3 belong to the range of hydrogenetic growth, whereas, zone 4, 5, 6, 7, 8, 9, and 10 belong to the range of mixed origin between hydrogenetic growth and early diagenetic growth. For U1406B-2 nodule, all zones belong to the range of hydrogenetic. All zones of U1365B-1 belong to the range of mixed origin between hydrogenetic growth and early diagenetic growth, whereas, U1365B-5 belong to the hydrogenetic growth. U1374-2 nodule, U1378-1 nodule, and U1399-5 nodule belong to the range of early diagenetic growth except for the zone 3 of U1399-5, which belong to the mixed origin.

Variations in each textural zone

The Mn/Fe, Ce/La, LREE/HREE, total REE and each chemical composition of each textural zone are plotted against the distance from surface. The each textural zones show low Mn/Fe of less than 1.65 and high SiO_2 contents of over than 15wt%, which indicate the high participation of terrigeneous materials into seawater and detrital grains during nodule growth. The usual criteria, Mn/Fe ratio of 2.5, for the distinction between hydrogenetic and early diagenetic origin seems not to be reasonable in this area, because it is very close to the source of terrigeneous materials and nodules are also distributed on the drift system.

Zone 1, 2, and 3 of U1398-1 nodule has Mn/Fe ratios higher than 1.1, whereas the other zones have Mn/Fe ratios lower than 1.1. Furthermore zone 1, 2, 3 and 4 of U1398-1 nodule have Cu+Ni+Zn contents more than 0.6wt%, however, the other zones have Cu+Ni+Zn contents less than 0.6wt%. The highest Co content of 0.45wt% is detected in zone 7&8 of U1373-2 nodule. Zone 9 and 10 of U1373-2 nodule and zone 5, 6, 7 and 8&9 of U1406B-2 nodule have high Co contents more than 0.2wt% compared to the other zones (Table 1).

The EPMA data were orderly presented into the graphs along the growth direction of the Fe-Mn-oxyhydroxide lamellae for each nodule. Fe contents are generally similar to Mn

contents except for U1398-1 nodule. Mn contents are much higher than Fe contents in U1398-1 nodule, which implies that most of the manganese oxyhydroxide phases in U1398-1 are crystalline buserite as confirmed by X-ray diffraction. Mn contents compared to Si+Al+K contents are generally high in U1398-1 and U1406B-2.

In zone 1, 2, 3, and 4 of U1373-2, Fe-vernadite is dominant, whereas Co and Mn-vernadite are dominant in zone 7 and 8. The contents of Cu+Ni+Zn are very high in U1398-1 nodule and in zone 4 and 5 of U1402-1 nodule. There is a Ni-dominant Mn-oxyhydroxide lamellae in zone 1 of U1406B-2, and a Cu-dominant lamellae in zone 5 of U1406B-2. Ba contents are high in Mn-oxyhydroxide lamellae of zone 4, 5, and 6 of U1402-1.

$^{10}Be/^{9}Be$ dating

The $^{10}Be/^{9}Be$ ages were calculated for the boundary of the textural zones using a 'best-fit' linear projection from core to surface of the sample on natural log plots of $^{10}Be/^{9}Be$ vs. depth. Outer layers of U1398-1 nodule show cuspate textures of early diagenetic origin and belongs to the Facies DH and/or DL. Inner layers show pseudocolumnar to laminated textures of hydrogenetic growth. Be dating reveals the growth rates of c. 3.5mm/My and age of c. 6.6Ma for early diagenetic growth in sediments. U1406B-2 nodule of Facies HH shows columnar textures of hydrogenetic growth, and has many interstitial detritals. Be dating reveals three different stages of growth and clustering of 12.6Ma. It shows the fast growth rate of 12.0mm/My from 12.6Ma to c. 11Ma, the intermediate growth rate of c. 5.7mm/My from c. 11Ma to c. 5.2Ma or c. 5.5Ma, and then the slow growth rate of 3.5mm/My.

U1373-2 and U1402-1 of Facies RH have asymmetric shapes and a distinct 'cap' or overgrowth on the upper hemisphere. The overgrowth seems to be originated from slow or zero growth of the lower hemisphere of the nodule during partial burial in sediments. The overgrowth layers show columnar and/or laminated textures of hydrogenetic growth, whereas the growth layers of S_b type nodule inside show cuspate/globular and/or parabolic cuspate textures with many microfossils and pores filled with detritals. The growth mechanism is uncertain yet, but might be originated from the mixed mechanism of hydrogenetic and biogenetic growth. Be dating reveals the clustering at c. 8.8Ma and c. 9.2Ma, and the fast growth rate of 9.7-9.8mm/My until c. 5.9Ma or c. 6.5Ma. After then they show the intermediate growth rates of 5mm/My to 8mm/My. The hydrogenetic overgrowths date back to 1.8Ma (U1402-1) or 0.4Ma (U1373-2).

Table 1. Characteristics of each textural zone for representative Fe-Mn nodules from Campbell Drift

Sample No.	Zone No.	Distance from surface (mm)	Thickness (mm)	Be-age* (Ma)	Fe-Mn oxide texture	Textural Genesis	Major Mn-Fe oxyhydroxides	Other major & minor minerals	Mn/Fe	Cu+Ni+Zn (wt%)	Co (wt%)	Region of REE pattern
U1373-2	1	0.0 - 2.9	2.9	0.37	Rectangular short columnar with microfossils	Hydrogenetic	Ver	Q, F, Px, Ap, Ilm, Amp	0.67	0.43	0.12	Hydrogenetic
	2	2.9 - 7.7	4.8	1.00	Large parabolic cuspates with many microfossils, pores filled with detritals	Biology dominant mixed	Ver	Q, F, Amp, Px, M	0.52	0.22	0.12	Hydrogenetic
	3	7.7 - 13.6	5.9	1.76								
	4	13.6 - 18.3	4.7	2.36			Ver	Q, F, Amp, M, Px	0.47	0.24	0.11	Mixed
	5	18.3 - 24.2	6.0	3.38	Parabolic cuspates with many microfossils, pores filled with detritals	Biology dominant mixed	Ver	Q, F, Amp, M, Ber, Px	0.51	0.22	0.16	Mixed
	6	24.2 - 30.2	5.9	4.57								
	7	30.2 - 35.4	5.3	5.64	Globular aggregates with pores	Mixed	Ver	Q, F, M, Amp, Ber, Px	0.77	0.25	0.45	Hydrogenetic
	8	35.4 - 39.5	4.1	6.47	Cuspates isolated by vertical cracks	Hydrogenetic						
	9	39.5 - 45.5	6.0	7.09	Cuspates with detritals	Hydrogenetic	Ver	Q, F, Px, Ber	0.65	0.23	0.30	Hydrogenetic
	10	45.5 - 54.6	9.0	8.01			Ver	Q, F, Ber, Px	0.50	0.21	0.22	Mixed
	11	54.6 - 62.1	7.5	8.79	Laminated to cuspates	Hydrogenetic	Ver	Q, F, Px, Ber	0.52	0.25	0.15	Mixed
U1398-1	1	0.0 - 6.4	6.42	1.98	Cuspates	Diagenetic	Bus, Ver	Q, F, Px	1.65	1.24	0.07	Diagenetic
	2	6.4 - 10.0	3.60	3.15	Cuspates	Diagenetic	Bus, Ver	Q, F, Px	1.51	1.24	0.10	Diagenetic
	3	10.0 - 14.0	3.96	4.93			Bus, Ver	Q, F, Px	1.11	0.87	0.13	Mixed
	4	14.0 - 18.7	4.69	6.56	Cuspates	Diagenetic	Bus, Ver	Q, F, Px	0.93	0.66	0.13	Mixed
	5	18.7 - 20.9	2.22		Pseudocolumnar to laminated	Mixed	Ver, Bus	Q, F, Px	1.02	0.74	0.12	Mixed
	6	20.9 - 21.5	0.61									
	core	30.9 - 32.9	1.98									
U1402-1	1	0.0 - 2.8	2.84	0.47	Flat-laminated to gently convex columar-layered	Hydrogenetic	Ver, Bus	Q, F	1.07	0.59	0.14	Hydrogenetic
	2	2.8 - 6.2	3.32	1.03			Ver	Q, F, Amp	0.95	0.39	0.14	Hydrogenetic
	3	6.2 - 10.5	4.35	1.76								
	4	10.5 - 16.5	5.97	2.76	Cuspates with detritals	Mixed	Bus, Ver	Q, F, Px, Amp	0.85	0.44	0.08	Mixed
	5	16.5 - 22.6	6.10	3.78	Cuspates with interstitial detritals	Biology dominant mixed	Bus, Ver	Q, F, Px, Amp	0.86	0.44	0.06	Mixed
	6	22.6 - 26.9	4.30	4.50								
	7	26.9 - 35.0	8.08	5.85	Cuspates showing dendritic growth	Biology dominant mixed	Ver	Q, F, Ber, Px	0.49	0.14	0.08	Mixed
	8	35.0 - 42.8	7.84	6.69								
	9	42.8 - 51.7	8.89	7.60								
	10	51.7 - 66.7	14.96	9.15	Undulatory laminated to pseudocolumnar	Mixed	Ver	Q, F, Ber, Px	0.46	0.15	0.07	Mixed
U1406B-2	1	0.0 - 4.2	4.18	1.19	Columnar-layered to slightly divergent columnar	Hydrogenetic	Ver	Q, Px, F	0.89	0.26	0.15	Hydrogenetic
	2	4.2 - 7.0	2.81	2.00			Ver	Q, F, Ap, Px	0.80	0.22	0.18	Hydrogenetic
	3	7.0 - 10.3	3.27	2.93			Ver	Q, Px, F	0.86	0.23	0.15	Hydrogenetic
	4	10.3 - 14.7	4.39	2.19			Ver	Q, F, Px	0.76	0.17	0.15	Hydrogenetic
	5	14.7 - 18.1	3.48	5.18			Ver	Q, F	0.78	0.17	0.22	Hydrogenetic
	6	18.1 - 26.7	8.55	6.78	Mostly columnar with many interstitial detritals, fan-like columar in the upper part	Hydrogenetic	Ver	Q, F, Px	0.75	0.15	0.20	Hydrogenetic
	7	26.7 - 36.1	9.47	6.78			Ver	Q, F, Px	0.82	0.19	0.25	Hydrogenetic
	8	36.1 - 40.8	4.65	8.45	Mostly columnar with many interstitial detritals, fan-like columar in the upper part	Hydrogenetic	Ver	Q, F, Px	0.76	0.17	0.21	Hydrogenetic
	9	40.8 - 51.5	10.69	9.27								
	10	51.5 - 58.4	6.92	11.01	Slightly divergent columnar	Hydrogenetic	Ver	Q, F, Px	0.57	0.15	0.12	Hydrogenetic
	11	58.4 - 64.2	5.80	11.59			Ver	Q, F, Ber	0.71	0.18	0.14	Hydrogenetic
	12	64.2 - 70.5	6.29	12.60								

*: Boundary ages of the textural zones, which were calculated from the results of Be^{10}/Be^{9} ratios analyzed by IGNS. Ver: Vernadite, Bus: Buserite, Q: Quartz, F: Feldspar, Px: Pyroxene, Ilm: Ilmenite, Amp: Amphibole, Ap: Apatite; Ber: Berthierine